

Article

Computational Flow Diverter Implantation—A Comparative Study on Pre-Interventional Simulation and Post-Interventional Device Positioning for a Novel Blood Flow Modulator

Maximilian Thormann ^{1,*}, Janneck Stahl ^{2,3,†} , Laurel Marsh ⁴, Sylvia Saalfeld ^{2,5}, Nele Sillis ¹, Andreas Ding ⁶, Anastasios Mpotsaris ⁷, Philipp Berg ^{2,8,†}  and Daniel Behme ^{1,2,†}

¹ Department of Neuroradiology, University Hospital Magdeburg, 39120 Magdeburg, Germany; nele.sillis@med.ovgu.de (N.S.); daniel.behme@med.ovgu.de (D.B.)

² Research Campus STIMULATE, University of Magdeburg, 39106 Magdeburg, Germany; janneck.stahl@ovgu.de (J.S.); sylvia.saalfeld@tu-ilmenau.de (S.S.); philipp.berg@ovgu.de (P.B.)

³ Department of Fluid Dynamics and Technical Flows, University of Magdeburg, 39106 Magdeburg, Germany

⁴ Department of Bioengineering, George Mason University, Fairfax, VA 22030, USA; lmarsh23@gmu.edu

⁵ Department of Computer Science and Automation, Ilmenau University of Technology, 98693 Ilmenau, Germany

⁶ Acandis GmbH, 75177 Pforzheim, Germany; ading@acandis.com

⁷ Department for Diagnostic and Interventional Radiology and Neuroradiology, Munich Clinic Harlaching, 81545 Munich, Germany; anastasios.mpotsaris@med.ovgu.de

⁸ Department of Medical Engineering, University of Magdeburg, 39106 Magdeburg, Germany

* Correspondence: maximilian.thormann@med.ovgu.de

† These authors contributed equally to this work.



Citation: Thormann, M.; Stahl, J.; Marsh, L.; Saalfeld, S.; Sillis, N.; Ding, A.; Mpotsaris, A.; Berg, P.; Behme, D. Computational Flow Diverter Implantation—A Comparative Study on Pre-Interventional Simulation and Post-Interventional Device Positioning for a Novel Blood Flow Modulator. *Fluids* **2024**, *9*, 55. <https://doi.org/10.3390/fluids9030055>

Academic Editor: Mesude Avci

Received: 28 December 2023

Revised: 5 February 2024

Accepted: 15 February 2024

Published: 23 February 2024



Copyright: © 2024 by the authors. Licensee MDPI, Basel, Switzerland. This article is an open access article distributed under the terms and conditions of the Creative Commons Attribution (CC BY) license (<https://creativecommons.org/licenses/by/4.0/>).

Abstract: Due to their effect on aneurysm hemodynamics, flow diverters (FD) have become a routine endovascular therapy for intracranial aneurysms. Since over- and undersizing affect the device's hemodynamic abilities, selecting the correct device diameter and accurately simulating FD placement can improve patient-specific outcomes. The purpose of this study was to validate the accuracy of virtual flow diverter deployments in the novel Derivo[®] 2 device. We retrospectively analyzed blood flows in ten FD placements for which 3D DSA datasets were available pre- and post-intervention. All patients were treated with a second-generation FD Derivo[®] 2 (Acandis GmbH, Pforzheim, Germany) and post-interventional datasets were compared to virtual FD deployment at the implanted position for implanted stent length, stent diameters, and curvature analysis using ANKYRAS (Galgo Medical, Barcelona, Spain). Image-based blood flow simulations of pre- and post-interventional configurations were conducted. The mean length of implanted FD was 32.61 (± 11.18 mm). Overall, ANKYRAS prediction was good with an average deviation of 8.4% ($\pm 5.8\%$) with a mean absolute difference in stent length of 3.13 mm. There was a difference of 0.24 mm in stent diameter amplitude toward ANKYRAS simulation. In vessels exhibiting a high degree of curvature, however, relevant differences between simulated and real-patient data were observed. The intrasaccular blood flow activity represented by the wall shear stress was qualitatively reduced in all cases. Inflow velocity decreased and the pulsatility over the cardiac cycle was weakened. Virtual stenting is an accurate tool for FD positioning, which may help facilitate flow FDs' individualization and assess their hemodynamic impact. Challenges posed by complex vessel anatomy and high curvatures must be addressed.

Keywords: computational stenting; flow diverter stent; intracranial aneurysm; hemodynamics

1. Introduction

Due to their effect on vessel blood flow and aneurysm hemodynamics, flow diverters (FDs) have become important and widely used instruments for the endovascular treatment of intracranial aneurysms with proven safety and effectiveness [1–3]. Using a fine braided mesh, they achieve high surface coverage and divert blood flow away from the aneurysm

along the axis of the parent vessel [4,5]. This process leads to progressive intra-aneurysmal thrombosis and neo-intima formation within the parent vessel, eventually causing complete hemodynamic decoupling between the parent vessel and aneurysm [6–8]. FDs are particularly used for complex, wide-neck aneurysms. Clinical trials evaluating FD effectiveness demonstrated encouraging outcomes, indicating high complete occlusion rates for treated aneurysms [1,2,9–14].

Selecting the correct device diameter affects the FD's ability to create adequate hemodynamic environments for aneurysm occlusion [15]. Both over- and undersizing the device alters its hemodynamic abilities. Yet sizing and correct deployment of FDs can be challenging due to irregular vessel anatomy and aneurysm location. Device implantation and predicting exact device location can be especially challenging in vessels with large caliber jumps or bifurcations. Not only anatomical characteristics but also technical maneuvers can affect the final size of the device. Vessel geometry and side branches must be carefully considered in pre-treatment planning [16]. Furthermore, FDs usually shorten when deployed. Manufacturers usually provide sizing support using landing zone diameters [17]. Different diameters of the proximal and distal landing zones and the high curvature of the parent vessel may lead to over- or undersizing of the device [18,19]. This sizing mismatch may cause insufficient wall apposition and alter bloodstream hemodynamics, reducing the device's ability to occlude the aneurysm or even leading to in-stent stenosis [18,20,21]. To date, correct sizing and implantation largely depend on the experience of the interventionalist.

In the future, individualized FDs may be designed using software tools based on the patient's vessel anatomy to achieve optimal outcomes [22]. Various strategies are available for virtual stent deployment in diverse aneurysm geometries [17,23–28]. Fast virtual stenting (FVS) methods are frequently used, as they account for the most relevant stent properties, balance numerical efforts, and have clinical applicability [29]. Research has examined FDs and their induced hemodynamic alterations using computational fluid dynamics (CFD) [30,31].

Narata et al. performed a retrospective validation study using ANKYRAS v2 software for several FD devices on 82 patients, including the first generation of the Derivo[®] device. They found a mean error between in-vivo implantation and simulations of 7.6% (SD 6.0%) [17]. In a recent preliminary study on 101 patients, Tong et al. used AneuGuide software, which applies a similar algorithm to ANKYRAS to simulate implantation with the pipeline embolization device. They found a mean simulation error of 6.2% with a good correlation between measured and simulated stent length [32]. Stent length measurements were performed on post-treatment 2D images. Consequently, measurements become dependent on projection and can potentially render simulation less precise in curvature vessels.

External validation results for 3D DSA simulations in a clinical setting are still limited. No solution has been able to adequately predict deployment dynamics [25].

The present study addresses these limitations by focusing on ten patients treated with a state-of-the-art embolization device. The Derivo[®] 2 flow diverter is a novel self-expanding device consisting of 48 nitinol wires that provide better X-ray visibility [33]. The second generation of the device was introduced in 2020 and provides better radiopacity due to a higher rate of platinum–iridium core. It has no distal or proximal device markers. The safety and efficacy of the Derivo[®] device have been shown in several studies [10,34–36]. Post-interventional data for Derivo[®] 2 show the desired flow redirection and activity reduction inside the aneurysm, which is beneficial for thrombosis formation with marked decreases in neck flow rate and mean inflow velocity [37].

Effective blood flow modulation requires reliable and fast virtual FD deployment methodologies. The purpose of this study was to compare the accuracy of patient-specific virtual stent deployment quantitatively and qualitatively against real 3D-DSA post-implantation results for the Derivo[®] 2 device. Image-based blood flow simulations of pre- and post-interventional configurations were conducted. Correct sizing and positioning were assessed, w.r.t. optimal blood flow modulation, and vascular geometry. Furthermore, hemodynamic assessments

of in-vivo FD deployments were performed and compared to the non-treated configuration to analyze the efficacy of the FD.

2. Materials and Methods

The study protocol was approved by the local ethics committee (Nr. 19/21). For each dataset, we compared in-vivo stent positions to virtual simulations using the commercially available ANKYRAS (Galgo Medical, Barcelona, Spain) software solution. Furthermore, numerical blood flow simulations were conducted based on pre- and post-interventional image data. Figure 1 illustrates the proposed workflow.

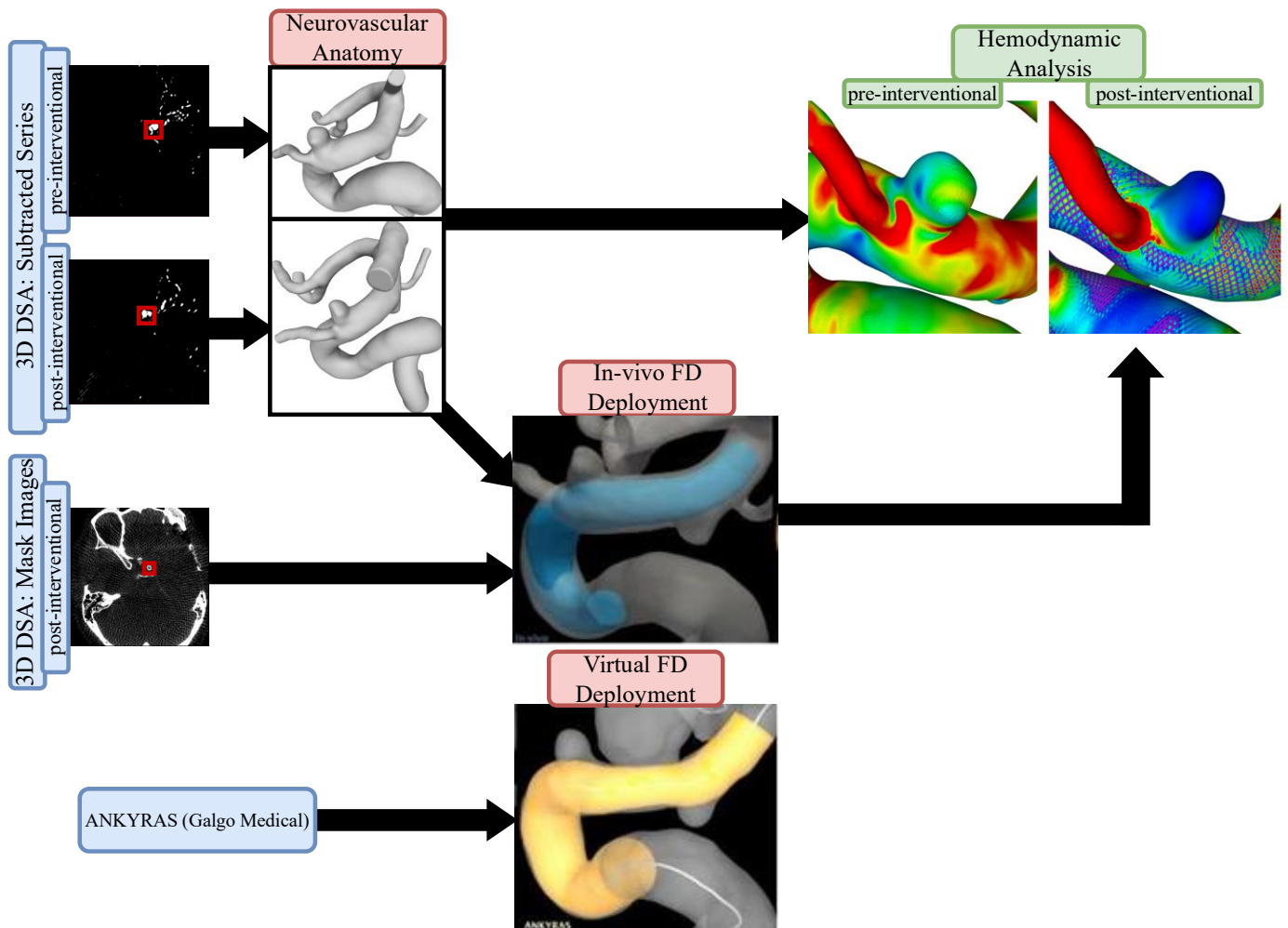


Figure 1. Flow chart of the presented workflow. Pre- and post-interventional images were used to extract the neurovascular anatomy as well as the in vivo FD deployment. Using a web-based application, virtual FD deployment was compared to the patient-specific in vivo FD. Hemodynamic comparisons were conducted based on pre- and post-interventional models (including patient-specific FD position) to investigate the resulting flow modulation effect.

2.1. Patients

We retrospectively analyzed FD implantations for intracranial aneurysms at the Department of Neuroradiology, University Hospital Magdeburg, Germany from December 2020 to May 2021. Complete 3D DSA datasets were available prior to and after the intervention. To allow for comparability, we only selected patients treated with the Derivo[®] 2 FD embolization device (DED, Acandis, Pforzheim, Germany). Post-interventional 3D datasets were compared to virtual stent implantations. Both ruptured and unruptured

cases were included. Interventionalists used 2D images to measure and define device size. Stent length, stent diameter, and curvature analysis were also compared.

We analyzed 10 out of 13 patients treated with DED for whom complete pre- and post-3D angiograms were available. Patient characteristics are provided in Table 1.

Table 1. Patient characteristics. ICA: internal carotid artery; MCA: middle cerebral artery.

Pat. Nr.	Sex	Age	Location	Morphology	Ruptured y/n	Aneurysm Size (mm) (Max-Neck-Dome)
1	female	67	ICA C6	saccular	n	10-7-14
2	male	54	Vertebral artery V4	saccular	n	2.5-5-5
3	female	63	ICA C7	blister	n	3-2-4
4	female	78	Posterior communicating artery	saccular	y	5.3-3.3-4.3
5	female	88	Posterior communicating artery	saccular	y	13.5-7-7.5
6	male	66	ICA C6	saccular	n	5-4-4
7	female	43	MCA M1/M2	saccular	n	2-2-2
8	female	49	ICA C7	dissecting	y	3-3.5-2.5
9	female	51	ICA C6	saccular	n	6-1.8-6.5
10	female	64	ICA C6	saccular	n	7-11-3.45

2.2. Image Acquisition

All treatments were performed using a flat-panel C-arm system (Axiom Artis Q, Siemens Healthcare, Erlangen, Germany). For pre- and post-implantation, 5 s 3D DSA was performed. FD size selection and deployment were performed by an interventional radiologist with over 10 years of experience. 3D datasets were calculated from a DynaCT performed in each case. An isotropic voxel resolution of 0.28 mm was used for all image acquisitions.

2.3. Segmentation

2.3.1. Neurovascular Anatomy

To segment patient-specific vascular structures based on 3D DSA data, MeVisLab (v3.4.1, MeVis Medical Solutions AG, Bremen, Germany) was used. Threshold-based methods and global Laplacian smoothing were used to obtain initial segmentation results. After converting the initial results into a 3D surface mesh, manual corrections were applied in the open-source 3D creation suite Blender (v2.9, Blender Foundations, Amsterdam, The Netherlands). Post-processing steps included the removal of artifacts from the surface mesh, separating incorrectly fused vessel sections, and optimizing the triangulated mesh. For maximum accuracy, the segmentations were assessed by an experienced interventional radiologist and created by a medical engineer with more than 3 years of experience in anatomical vessel segmentation. These steps were performed for all 10 patients based on pre- and post-interventional 3D DSA data, resulting in 20 patient-specific 3D models (see Figure 2).

2.3.2. In Vivo Flow Diverter Deployment

To obtain the exact position and shape of the implanted flow diverter stent, a mask series of post-interventional 3D DSA datasets was used. Based on these images, 3D models representing the deployed stent were extracted using threshold-based segmentation methods implemented in MeVisLab. Enveloped surfaces indicating the in vivo stenting results were subsequently used to reconstruct the real stent within the vascular structures.

2.4. Virtual Stenting

The web-based application ANKYRAS (Galgo Medical, Barcelona, Spain) was used to simulate FD deployments and comparisons with real FD deployments. The user can select

a patient-specific FD size (recall Table 2) and indicate the desired stent position. Based on the segmented surface meshes, the algorithm analyzes the local morphological features of the lumen. Therefore, the vessels' centerline was calculated as well as the vessel diameters of discrete sections based on the diameter of the maximum inscribed spheres. The nominal FD configurations were deployed starting at the distal endpoints. The algorithm calculates the proportion of nominal FD length required for vessel wall adaptation based on vessel morphology. Depending on the local vessel caliber and curvature, the underlying length change function considers the foreshortening effect of the virtual device. This results in a three-dimensional deformed surface representing actual FD geometry and is applicable within seconds to ensure clinical usability. We recommend interested readers to Fernandez et al. [38] for further details on the virtual stenting algorithm.

2.5. Image-Based Blood Flow Simulation

Segmented surface mesh models of neurovascular anatomy (see Figure 2) were converted into volume meshes using polyhedral and prism cells (three layers at the outer wall) with a mean base size of 0.2 mm. To represent FD treatment within the hemodynamic simulation, an in-house-developed FVS tool [39] was applied. The Derivo[®] 2 FD's morphological properties were obtained using nominal stent parameters provided by the manufacturer. Furthermore, the extracted in vivo deployment allowed patient-specific positioning for each FD. The generated virtual FDs were also spatially discretized using polyhedral cells. A small base size of 0.02 mm was used for remeshing to properly resolve all stent struts. Transient numerical simulations were conducted using the finite-volume-based solver StarCCM+ (v15, Siemens PLM Software Inc., Plano, TX, USA). Since no patient-specific flow information was available, representative flow waveforms were applied to the inlet cross-sections, according to Durka et al. [40]. For multiple outlets, an advanced in-house flow-splitting algorithm was used [41]. In all twenty configurations, blood was treated as an incompressible ($\rho = 1055 \text{ kg/m}^3$) and Newtonian fluid ($\eta = 4 \text{ mPa s}$). Furthermore, rigid walls as well as a laminar flow behavior were assumed.

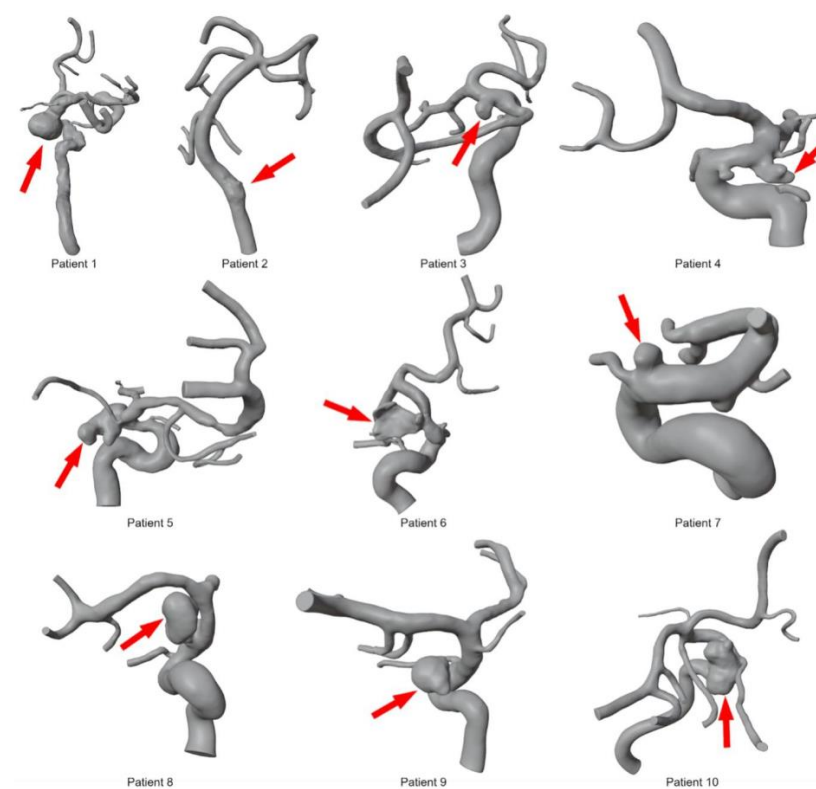


Figure 2. Overview of segmented 3D models for ten intracranial aneurysms before deployment of the FD stents. The red arrow indicates the location of each aneurysm.

Table 2. Quantitative comparison of virtual and real deployment lengths in 10 patient-specific cases. Notice the sufficient agreement with a slight overestimation of the pre-interventional planning tool in almost all patients (FD = Flow Diverter).

Patient	FD Size	In Vivo- Length	Virtual Length	% Δ
01	5.5 × 30	58.6	47.08	−20%
02	5 × 25	38.9	39.71	2%
03	5 × 25	34.66	37.84	9%
04	5 × 20	31.818	33.71	6%
05	5 × 20	37.42	43.04	15%
06	5 × 15	30.56	32.21	5%
07	4 × 20	29.33	32.6	11%
08	4 × 15	22.5	23.686	5%
09	4 × 15	22.48	24.51	9%
10	3.5 × 15	19.85	19.66	−1%

2.6. Quantitative and Quantitative Analysis

When reconstructed from 3D DSA, each stent provides an enveloped surface on which the individual stent struts are not resolved. Due to the limited resolution of the imaging modality, this envelope is thicker than the actual tine diameter. Therefore, a median surface was created using StarCCM+ in which the outer and inner surfaces were translated towards one another until contact was achieved. This process allowed the diameter of the deployed in vivo stent to be calculated. VMTK (v1.4.0, vmtk.org) was employed to extract the centerline and diameter of the stent and corresponding vessel. All data analyses were performed with MATLAB (v9.9, MathWorks, Natick, MA, USA). These results were compared to those of commercially available software.

To investigate the FD-induced flow modulation effect, the time-averaged wall shear stress (AWSS) was calculated [42] to describe the tangential stress against the luminal wall. In addition, the velocity at the ostium’s inflow area was extracted.

3. Results

Implanted Derivo® 2 FDs had a mean length of 32.61 mm (±11.18 mm). Overall agreement between virtual and real deployment lengths of the analyzed cases was high with a mean deviation of 8.4% (±5.8%) in the ANKYRAS simulation compared to in vivo stent sizes. In 8/10 patients, sizing was slightly over-predicted with a mean of 9%. In 2/10 patients, the software slightly underestimated the stent length. The mean diameter amplitude for implanted stents was 1.75 mm and 1.99 mm in simulation. The values for in vivo stent position, virtual simulation, and stent diameters are summarized in Tables 2 and 3.

Table 3. Quantitative comparison of real and virtual deployment stent diameters for ten patient-specific cases. Overall, a slight overestimation of diameter amplitude is seen in the simulation.

Patient	Location	Stent Diameter (mm)	
		Virtual Simulation	In Vivo
01	Proximal	3.77	3.46
	Min–Max	2.09–4.55	2.82–5.67
	Distal	2.6	2.36
	Aneurysm	4.55	5.67
02	Proximal	3.66	4.39
	Min–Max	3.51–4.27	3.51–5.15
	Distal	3.57	3.61
	Aneurysm	4.14	5.15

Table 3. Cont.

Patient	Location	Stent Diameter (mm)	
		Virtual Simulation	In Vivo
03	Proximal	4.13	4.32
	Min–Max	3.17–5.23	2.30–4.71
	Distal	3.17	2.67
	Aneurysm	3.58	2.88
04	Proximal	3.02	3.88
	Min–Max	2.19–4.61	2.67–4.33
	Distal	2.59	3.45
	Aneurysm	2.44/2.36	3.48
05	Proximal	3.94	4.12
	Min–Max	1.42–4.11	0.92–4.12
	Distal	1.52	1.03
	Aneurysm	3.11	3.71
06	Proximal	3.47	4.15
	Min–Max	1.05–3.66	1.71–4.15
	Distal	--	2.03
	Aneurysm	1.41	2.93
07	Proximal	2.54	3.83
	Min–Max	2.54–3.58	2.37–3.83
	Distal	2.6	2.95
	Aneurysm	3.19/2.68	3.11/2.85
08	Proximal	3.52	3.91
	Min–Max	2.66–4.11	2.18–4.14
	Distal	2.75	2.89
	Aneurysm	3.32	4.14
09	Proximal	3.43	3.23
	Min–Max	3.03–3.69	2.73–3.7
	Distal	3.27	3.34
	Aneurysm	3.69	3.7
10	Proximal	--	3.48
	Min–Max	2.10–3.40	2.34–3.62
	Distal	3.36	2.58
	Aneurysm	2.65	3.62

Case 1 had the greatest deviation from in vivo stent size, with ANKYRAS underestimating stent length by 20%. The patient’s vasculature in this case had a significant level of pathological dilatation, making it difficult to produce a virtual file for stent placement. Since the anterior cerebral artery’s (ACA) distal outlet was not properly segmented, the simulation did not allow for precise FD placement. While in vivo, the FD’s distal end had to be placed in the proximal MCA due to excessive curvature. Virtual stenting could not be precisely reproduced because of the relatively low quality of segmentation.

Cases 5 and 7 showed relatively high extension in the simulation. Case 5 had the second-highest deviation from in vivo length. The vessel exhibited high curvature and severe stenosis proximal to the aneurysm. There was a high caliber jump between the proximal and distal diameters, from 1.42 mm to 4.11 mm (Table 3). ANKYRAS segmentation showed a stenosis at the distal stent landing zone, which artificially lengthened the stent. The vessel diameter covered by the stent was 3.12 mm on average. By comparison, the ANKYRAS segmentation had an average diameter of 2.48 mm. This difference was a major contributor to the exaggerated prediction. Case 7 had two small aneurysms and two FD had to be implanted. The placement of the first FD was too proximal; therefore, a second one was placed distally to cover both small aneurysms. The vessel exhibited a high curvature with 1/4 of the stent’s length experiencing this curvature (>0.2 R).

Case 4 had two aneurysms and an over-prediction of length by 11%. The vessel diameter was smaller than expected for a 5 mm stent, potentially caused by size unavailability. The software significantly oversized the stent distally. It is possible that ANKYRAS could not capture significant stretching caused by the contraction of the stent.

Cases 2, 6, and 8 showed good agreement between in vivo sizing and software simulation. Case 2 had only a minor difference of 2% from the in vivo size. The vessels exhibited the lowest curvature of all 10 patients. There was a minimal caliber jump between the proximal and distal diameters in the simulation (Table 3). A minor disagreement of 5% was observed between cases 6 and 8 with the in vivo size. Both showed a very low curvature. In case 6, the vessel had a flattened cross-sectional shape at and distal to the aneurysm, which compressed and lengthened the stent. The caliber jump between the proximal and distal diameter was 2.61 mm. Case 8 showed no vessel stenosis or other pathology.

In cases 3 and 9, the software simulation deviated by 9% from the in vivo stent size. The vessel in case 9 underwent a sharp bend due to high curvature. Nevertheless, strong agreement with the simulation was seen. Case 3 exhibited an average internal carotid artery (ICA) curvature. Compared to other cases, it seems as though the stent straightened the distal ICA (Figure 3), which may explain the disagreement in size.

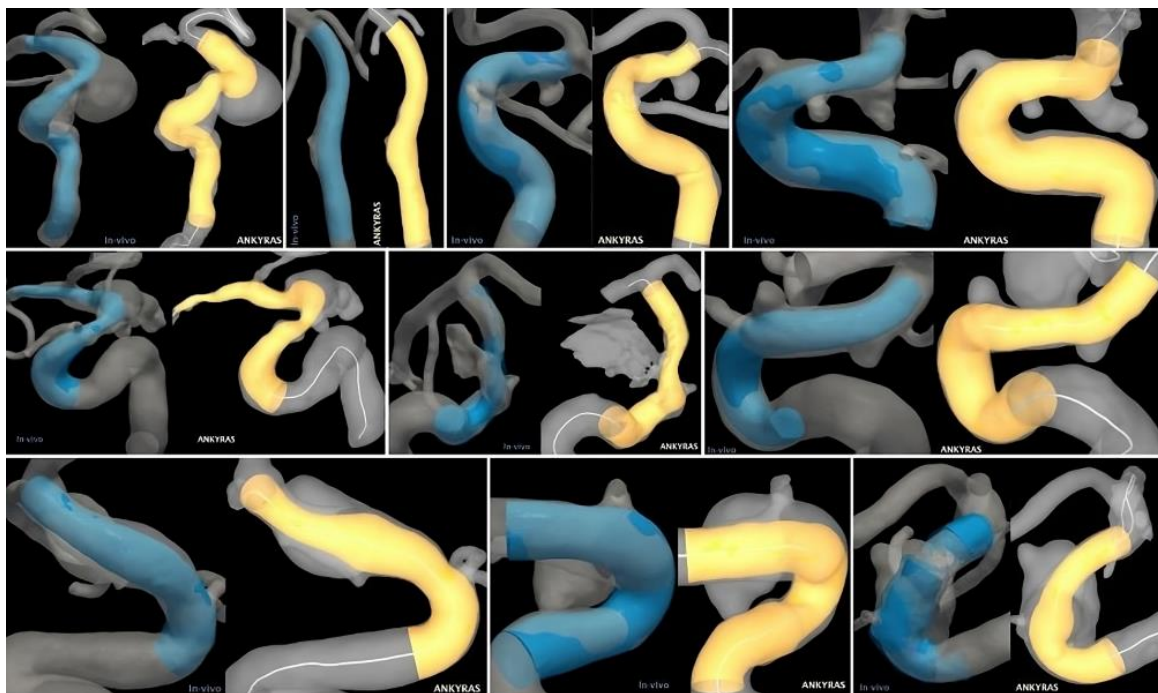


Figure 3. Qualitative comparison of in vivo (left/blue) and virtual (right/yellow) stenting results for all ten patient-specific intracranial aneurysms.

Hemodynamic simulations of the pre- and post-interventional state allow us to investigate the flow modulation effect due to the deployed FD. Figure 4 shows their effect on the AWSS at the luminal vessel walls of the aneurysm sac. It is qualitatively visible that all cases show decreasing shear stresses after deployment. This effect is most evident in cases 6 and 9, whereas cases 1 and 4 show a moderate reduction. In cases 5 and 10, a strong reduction in the AWSS in the distal area of the aneurysm dome is apparent. However, there are still noticeably increased shear stresses in the entrance area close to the ostium.

In Figure 5, the flow modulation effect is perceived with respect to the velocity at the ostium inflow area. Here, all cases exhibit a reduction in velocity magnitude after FD deployment. For cases 1 and 2, the slowdown of the flow is the lowest. Moreover, a homogenization of velocity curves over time is visible in all other cases.

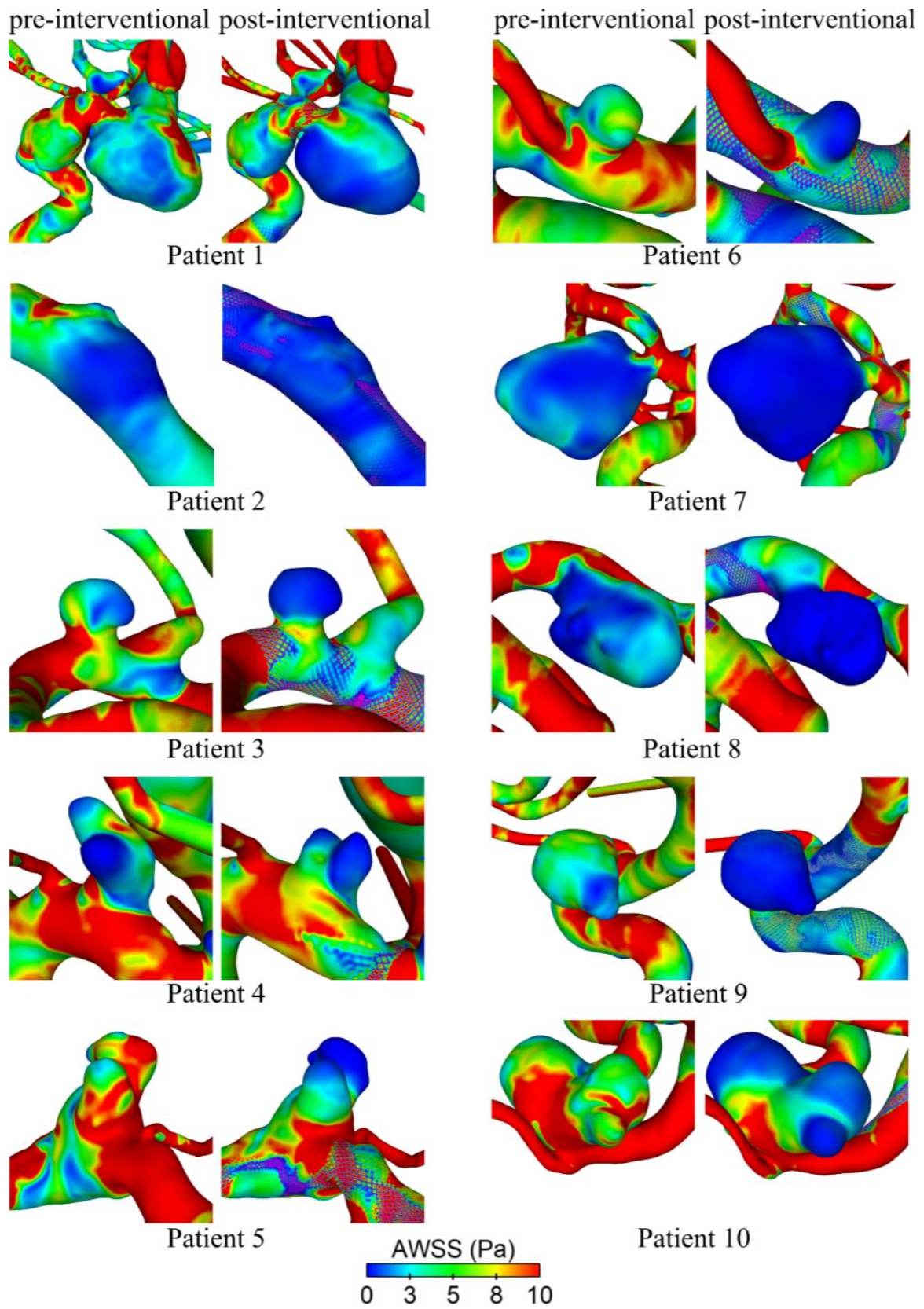


Figure 4. Qualitative comparison of time-averaged wall shear stress (AWSS) on the luminal surface before (pre-interventional) and after (post-interventional) FD treatment for all ten patients.

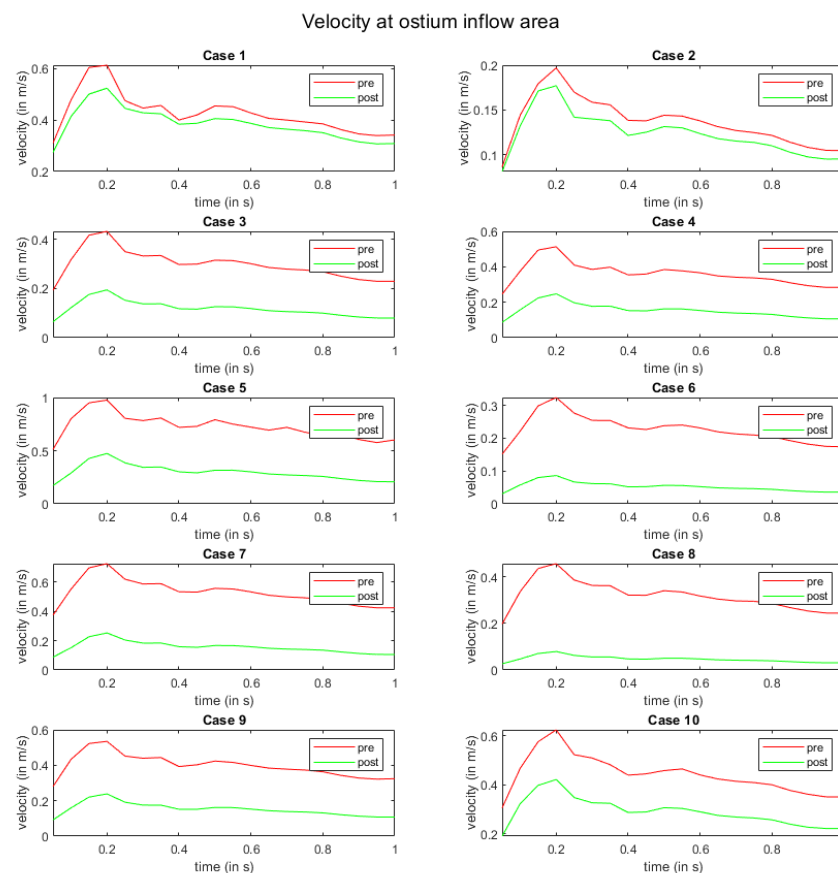


Figure 5. Time-dependent inflow velocity at the ostium area over one cardiac cycle. The red and green curves indicate pre- and post-interventional states, respectively.

4. Discussion

FDs do not physically exclude the intracranial aneurysm from blood flow but create hemodynamic conditions to trigger thrombosis and remodeling. Therefore, correct aneurysm deployment of FDs is key to inducing intra-aneurysmal blood flow changes. The hemodynamic effects of FDs, as well as metal coverage along the parent arterial segment, are significantly influenced by the interplay between the nominal dimensions of the device and those of the parent vessel [17]. Thus, choosing the correct size affects the device's hemodynamic abilities. Undersizing can result in poor wall apposition and insufficient coverage of the aneurysm ostium and hyperplasia of the intima [19,21,43]. On the contrary, oversizing may lead to inefficient aneurysm occlusion and in-stent stenosis [15]

In this study, we examined the accuracy of virtual FD implantation by comparing in vivo stent positions to virtual simulations using the commercially available ANKYRAS software solution. We investigated FD implantation for ruptured and unruptured intracranial aneurysms in 10 patients using the novel Derivo[®] 2 device. Our goal was to validate the precision of FD length and diameter, as predicted by the software. Simulations based on pre-interventional angiograms were compared to rarely available post-interventional implantation characteristics. Furthermore, we analyzed treatment-related flow modulation effects using hemodynamic simulations based on patient-specific post-interventional FD positions.

In our dataset, the overall agreement between the software simulation and in vivo stent size was clinically sufficient, with an average deviation in length of 8.4% in the simulated cases. The software tended to be more accurate in low-curvature vessels. In vessels exhibiting a high degree of curvature, however, relevant differences between the simulated and real-patient data were observed. The average deviation of the implanted length was 3.13 mm (SD \pm 3.32 mm), which is in line with Kellermann et al. [21]. However,

we did not need the co-registration of flat panel CT images to co-register images, which is a main limitation in Kellermann's study. A slight overestimation of diameter amplitude was seen in the simulation.

Choosing the correct size for FD deployment is crucial for intra-aneurysm hemodynamic effects. However, sizing can be challenging even for experienced interventionalists. Stent foreshortening can lead to relevant differences between nominal and implanted device sizes, which can be modified by the interventionalist through device manipulation during the procedure. Therefore, foreshortening is not only influenced by the stent or FD design but also highly depends on the deployment mode. In everyday clinical practice, a deviation between the nominal and implanted length of a few millimeters is considered acceptable, at least in traditional stenting or FD placement. However, the tolerance level depends on vessel anatomy. If the FD is implanted proximally or distally in a branching vessel or large vessel curvature, a higher accuracy of 1–2 mm is desirable. In other cases, a higher deviation from *in vivo* sizing may be acceptable. Our study shows that the software delivers more precise length prediction in smaller vessels, without complex vessel anatomy, as there is less stent extension regardless of curvature.

One limitation of the simulation tool employed in this study is that adjusting the landing zone or device positioning is not possible. While such simulations prove clinically sufficient in most treated cases, they may fall short in scenarios involving patients with compounded vessel pathologies or curvatures. The ability to modify these parameters becomes particularly crucial in ensuring more accurate length predictions. One example from our dataset is case 1, where the vessel exhibited a high level of pathological dilation, causing difficulty in the stent deployment simulation. In such instances, adapting the landing zone and device positioning may contribute to a more precise simulation and address the complexities introduced by certain anatomical features.

Other studies have noted the advantages of virtual stenting in device selection [18]. The technical approaches to virtual stenting described here are very different. Generally, a compromise between modeling accuracy and computational effort must result in varying stenting possibilities. Techniques based on the finite-element method allow for precise consideration of deformation behavior (including stent release and stent–wall interaction) and considerable simulation times are required, heavily limiting clinical applicability [32,44]. Other so-called FVS approaches are based on active contours or free-form deformations employing representatives of the actual braided stent structures [26]. The ANKYRAS software chosen in this study is associated with this class of algorithms. We recommend the interested reader to Berg et al. [45] for more information on the advantages and disadvantages of different virtual stenting techniques.

Even if software simulation is not widely used in clinical practice today, future advancements in FD design, such as individualized proximal and distal stent diameters or changing braiding angles, will necessitate the development of software tools that adequately and reliably predict stent positioning. As a result, estimation accuracy becomes extremely important. Our findings revealed that prediction heavily depends on segmentation quality, and that sizing becomes increasingly erroneous with complex vascular architecture. These issues must be addressed in future software designs before the tools can be employed in the clinical planning of customized devices.

The analysis of pre- and post-3D DSA data in our study adds significantly to data accuracy because no 2D/3D co-registration step was necessary for enabling 3D images or data comparison in the same segmented dataset.

The conducted hemodynamic simulations allowed us to investigate the desired flow reduction efficacy. The AWSS decrease in all cases indicated reduced intraluminal flow activities, yielding the desired occlusion of the aneurysms (Figure 4). Reduced inflow velocities also showed the slowdown of the flow due to the FD (recall Figure 5). The hemodynamic results are in line with the findings of Kulscar et al. and Dholakia et al., concluding that such conditions are necessary for thrombosis formation [46,47].

As highlighted earlier, challenging anatomical features or segmentation issues can contribute to inaccurate simulation outcomes, elucidating the minimal disparities in velocities observed at the ostium inflow area in case 1 (Figure 5). It is important to acknowledge that intricate anatomical configurations, such as those encountered in case 2 (involving post-dissection aneurysms), where identifying the ostium itself can pose challenges, may also be associated with simulation difficulties. In instances similar to these cases, the simulation results may be influenced by complexities in the anatomical structure. However, it is noteworthy that despite these specific cases, the simulations conducted on a diverse range of anatomies consistently produced highly accurate and plausible results, reinforcing the methodology's reliability across various scenarios.

The major limitations of our analysis are the low number of cases and the retrospective design of the study. Due to the novelty of the Derivo[®] 2 device, the number of treated cases is still limited. Furthermore, segmentation results influence virtual stenting since segmentation parameters might change vessel diameters [48]. In addition, no virtual stenting tool can currently model manipulation steps during FD implantation initiated by the interventionalist. However, these stent deployment techniques (pushing/pulling) can significantly influence the length of braided stents and implantation results. Furthermore, the blood flow simulations show limitations with respect to the selected boundary conditions, e.g., for the inflow curves, representative values were selected from the literature. These conditions may not reproduce the effects of organs and vessels outside the simulated region [49,50].

5. Conclusions

Our validation analysis shows that virtual simulation of stent implantation is a clinically sufficient and accurate tool for FD implantation and post-implantation flow modulation that helps interventionalists achieve optimal results in clinical practice. We demonstrated the robustness of the simulation methodology across a diverse range of anatomies. Our study sheds light on potential limitations associated with challenging anatomies while underscoring the overall reliability and applicability of the simulation approach. Future refinements in segmentation techniques and simulation algorithms could further enhance the accuracy of results. Simulation may assist device selection by fully exploiting FDs' intra-aneurysmal hemodynamic effects.

Author Contributions: Conceptualization, M.T., S.S., A.M., P.B. and D.B.; Data curation, M.T., L.M., J.S., N.S., A.D., P.B. and D.B.; Formal analysis, M.T., L.M., J.S. and N.S.; Funding acquisition, D.B.; Investigation, M.T., J.S., N.S., P.B. and D.B.; Methodology, M.T., L.M. and J.S.; Project administration, P.B. and D.B.; Resources, L.M., S.S., A.M., P.B. and D.B.; Software, J.S., S.S. and A.D.; Supervision, P.B. and D.B.; Validation, M.T., L.M., J.S., S.S., A.M., N.S., P.B. and D.B.; Visualization, L.M., J.S. and N.S.; Writing—original draft, M.T., L.M. and P.B.; Writing—review and editing, M.T., L.M., J.S., S.S., A.M., N.S., P.B. and D.B. All authors have read and agreed to the published version of the manuscript.

Funding: This work was partly funded by the Federal Ministry of Education and Research in Germany within the Research campus STIMULATE (Grant Number 13GW0473A). Furthermore, the financial support of the DFG (Deutsche Forschungsgemeinschaft) for J.S. within the project SPP2311 “Robust Coupling of Continuum-biomechanical In Silico Models to Establish Active Biological System Models for Later Use in Clinical Applications—Co-design of Modelling, Numerics and Usability” (project number: 465189657) is gratefully acknowledged.

Data Availability Statement: The datasets used and/or analyzed during the current study are available from the corresponding author upon reasonable request.

Acknowledgments: Technical advice was provided by Christina Dill, Acandis GmbH, Pforzheim, Germany.

Conflicts of Interest: The authors declare no conflict of interest.

Abbreviations

ACA	Anterior cerebral artery
AWSS	Time-averaged wall shear stress
ICA	Internal carotid artery
FD	Flow diverter
FVS	Fast virtual stenting
DSA	Digital subtraction angiography
DED2	Derivo [®] 2 flow diverter embolization device
MCA	Middle cerebral artery

References

1. Brinjikji, W.; Murad, M.H.; Lanzino, G.; Cloft, H.J.; Kallmes, D.F. Endovascular Treatment of Intracranial Aneurysms with Flow Diverters: A Meta-Analysis. *Stroke* **2013**, *44*, 442–447. [[CrossRef](#)]
2. Taschner, C.A.; Stracke, C.P.; Dorn, F.; Kadziolka, K.B.; Kreiser, K.; Solymosi, L.; Pham, M.; Buhk, J.H.; Turowski, B.; Reith, W.; et al. Derivo Embolization Device in the Treatment of Unruptured Intracranial Aneurysms: A Prospective Multicenter Study. *J. Neurointerv. Surg.* **2021**, *13*, 541–546. [[CrossRef](#)] [[PubMed](#)]
3. Martínez-Galdámez, M.; Biondi, A.; Kalousek, V.; Pereira, V.M.; Ianucci, G.; Gentric, J.C.; Mosimann, P.J.; Brisbois, D.; Schob, S.; Quäschling, U.; et al. Periprocedural Safety and Technical Outcomes of the New Silk Vista Baby Flow Diverter for the Treatment of Intracranial Aneurysms: Results from a Multicenter Experience. *J. Neurointerv. Surg.* **2019**, *11*, 723–727. [[CrossRef](#)] [[PubMed](#)]
4. Möhlenbruch, M.A.; Kizilkilic, O.; Killer-Oberpfalzer, M.; Baltacioglu, F.; Islak, C.; Bendszus, M.; Cekirge, S.; Saatci, I.; Kocer, N. Multicenter Experience with FRED Jr Flow Re-Direction Endoluminal Device for Intracranial Aneurysms in Small Arteries. *AJNR Am. J. Neuroradiol.* **2017**, *38*, 1959. [[CrossRef](#)] [[PubMed](#)]
5. Voigt, P.; Schob, S.; Jantschke, R.; Nestler, U.; Krause, M.; Weise, D.; Lobsien, D.; Hoffmann, K.T.; Quäschling, U. Stent-Assisted Coiling of Ruptured and Incidental Aneurysms of the Intracranial Circulation Using Moderately Flow-Redirecting, Braided Leo Stents-Initial Experience in 39 Patients. *Front. Neurol.* **2017**, *8*, 602. [[CrossRef](#)] [[PubMed](#)]
6. Kadirvel, R.; Ding, Y.H.; Dai, D.; Rezek, I.; Lewis, D.A.; Kallmes, D.F. Cellular Mechanisms of Aneurysm Occlusion after Treatment with a Flow Diverter. *Radiology* **2014**, *270*, 394–399. [[CrossRef](#)] [[PubMed](#)]
7. Briganti, F.; Leone, G.; Marseglia, M.; Mariniello, G.; Caranci, F.; Brunetti, A.; Maiuri, F. Endovascular Treatment of Cerebral Aneurysms Using Flow-Diverter Devices: A Systematic Review. *Neuroradiol. J.* **2015**, *28*, 365–375. [[CrossRef](#)] [[PubMed](#)]
8. Ravindran, K.; Salem, M.M.; Alturki, A.Y.; Thomas, A.J.; Ogilvy, C.S.; Moore, J.M. Endothelialization Following Flow Diversion for Intracranial Aneurysms: A Systematic Review. *Am. J. Neuroradiol.* **2019**, *40*, 295–301. [[CrossRef](#)]
9. Puffer, R.C.; Piano, M.; Lanzino, G.; Valvassori, L.; Kallmes, D.F.; Quilici, L.; Cloft, H.J.; Boccardi, E. Treatment of Cavernous Sinus Aneurysms with Flow Diversion: Results in 44 Patients. *AJNR Am. J. Neuroradiol.* **2014**, *35*, 948. [[CrossRef](#)] [[PubMed](#)]
10. Trivelato, F.P.; Abud, D.G.; Ulhôa, A.C.; Waihrich, E.S.; Abud, T.G.; Castro Afonso, L.H.; Nakiri, G.S.; De Castro, G.D.; Parente, B.D.S.M.; Dos Santos Silva, R.; et al. Derivo Embolization Device for the Treatment of Intracranial Aneurysms. *Stroke* **2019**, *50*, 2351–2358. [[CrossRef](#)]
11. Monteiro, A.; Burke, S.M.; Baig, A.A.; Khan, S.; Cappuzzo, J.M.; Waqas, M.; Dietrich, J.E.; Levy, E.L.; Siddiqui, A.H. A Systematic Review and Meta-Analysis of the Derivo Embolization Device: A Novel Surface-Modified Flow Diverter for Intracranial Aneurysm Treatment. *J. Neurointerv. Surg.* **2022**, *14*, 1125–1129. [[CrossRef](#)] [[PubMed](#)]
12. Bonafe, A.; Perez, M.A.; Henkes, H.; Lylyk, P.; Bleise, C.; Gascou, G.; Sirakov, S.; Sirakov, A.; Stockx, L.; Turjman, F.; et al. Diversion-P64: Results from an International, Prospective, Multicenter, Single-Arm Post-Market Study to Assess the Safety and Effectiveness of the P64 Flow Modulation Device. *J. Neurointerv. Surg.* **2022**, *14*, 898–903. [[CrossRef](#)] [[PubMed](#)]
13. Becske, T.; Kallmes, D.F.; Saatci, I.; McDougall, C.G.; Szikora, I.; Lanzino, G.; Moran, C.J.; Woo, H.H.; Lopes, D.K.; Berez, A.L.; et al. Pipeline for Uncoilable or Failed Aneurysms: Results from a Multicenter Clinical Trial. *Radiology* **2013**, *267*, 858–868. [[CrossRef](#)] [[PubMed](#)]
14. Killer-Oberpfalzer, M.; Kocer, N.; Griessenauer, C.J.; Janssen, H.; Engelhorn, T.; Holtmannspötter, M.; Buhk, J.H.; Finkenzeller, T.; Fesl, G.; Trenkler, J.; et al. European Multicenter Study for the Evaluation of a Dual-Layer Flow-Diverting Stent for Treatment of Wide-Neck Intracranial Aneurysms: The European Flow-Redirection Intraluminal Device Study. *AJNR Am. J. Neuroradiol.* **2018**, *39*, 841–847. [[CrossRef](#)] [[PubMed](#)]
15. Mut, F.; Cebral, J.R. Effects of Flow-Diverting Device Oversizing on Hemodynamics Alteration in Cerebral Aneurysms. *AJNR Am. J. Neuroradiol.* **2012**, *33*, 2010–2016. [[CrossRef](#)]
16. Iosif, C.; Berg, P.; Ponsonnard, S.; Carles, P.; Saleme, S.; Ponomarjova, S.; Pedroló-Silveira, E.; Mendes, G.A.C.; Waihrich, E.; Trolliard, G.; et al. Role of Terminal and Anastomotic Circulation in the Patency of Arteries Jailed by Flow-Diverting Stents: From Hemodynamic Changes to Ostia Surface Modifications. *J. Neurosurg.* **2017**, *126*, 1702–1713. [[CrossRef](#)]
17. Narata, A.P.; Blasco, J.; Roman, L.S.; Macho, J.M.; Fernandez, H.; Moyano, R.K.; Winzenrieth, R.; Larrabide, I. Early Results in Flow Diverter Sizing by Computational Simulation: Quantification of Size Change and Simulation Error Assessment. *Oper. Neurosurg.* **2018**, *15*, 557–566. [[CrossRef](#)]

18. Ospel, J.M.; Gascou, G.; Costalat, V.; Piergallini, L.; Blackham, K.A.; Zumofen, D.W. Comparison of Pipeline Embolization Device Sizing Based on Conventional 2D Measurements and Virtual Simulation Using the Sim&Size Software: An Agreement Study. *AJNR Am. J. Neuroradiol.* **2019**, *40*, 524. [[CrossRef](#)] [[PubMed](#)]
19. Berg, P.; Iosif, C.; Ponsonnard, S.; Yardin, C.; Janiga, G.; Mounayer, C. Endothelialization of Over- and Undersized Flow-Diverter Stents at Covered Vessel Side Branches: An in Vivo and in Silico Study. *J. Biomech.* **2016**, *49*, 4–12. [[CrossRef](#)] [[PubMed](#)]
20. Bing, F.; Darsaut, T.E.; Salazkin, I.; Makoyeva, A.; Gevry, G.; Raymond, J. Stents and Flow Diverters in the Treatment of Aneurysms: Device Deformation In Vivo May Alter Porosity and Impact Efficacy. *Neuroradiology* **2013**, *55*, 85–92. [[CrossRef](#)]
21. Kellermann, R.; Serowy, S.; Beuing, O.; Skalej, M. Deployment of Flow Diverter Devices: Prediction of Foreshortening and Validation of the Simulation in 18 Clinical Cases. *Neuroradiology* **2019**, *61*, 1319–1326. [[CrossRef](#)]
22. Velvaluri, P.; Pravdivtseva, M.S.; Berg, P.; Wodarg, F.; Lima De Miranda, R.; Hövener, J.-B.; Jansen, O.; Quandt, E.; Velvaluri, P.; Quandt, E.; et al. Thin-Film Patient-Specific Flow Diverter Stents for the Treatment of Intracranial Aneurysms. *Adv. Mater. Technol.* **2021**, *6*, 2100384. [[CrossRef](#)]
23. Bouillot, P.; Brina, O.; Yilmaz, H.; Farhat, M.; Erceg, G.; Lovblad, K.O.; Vargas, M.I.; Kulcsar, Z.; Pereira, V.M. Virtual-versus-Real Implantation of Flow Diverters: Clinical Potential and Influence of Vascular Geometry. *Am. J. Neuroradiol.* **2016**, *37*, 2079–2086. [[CrossRef](#)]
24. Larrabide, I.; Kim, M.; Augsburg, L.; Villa-Uriol, M.C.; Rüfenacht, D.; Frangi, A.F. Fast Virtual Deployment of Self-Expandable Stents: Method and In Vitro Evaluation for Intracranial Aneurysmal Stenting. *Med. Image Anal.* **2012**, *16*, 721–730. [[CrossRef](#)] [[PubMed](#)]
25. Závodszy, G.; Csippa, B.; Paál, G.; Szikora, I. A Novel Virtual Flow Diverter Implantation Method with Realistic Deployment Mechanics and Validated Force Response. *Int. J. Numer. Method Biomed. Eng.* **2020**, *36*, e3340. [[CrossRef](#)] [[PubMed](#)]
26. Lamooki, S.R.; Tutino, V.M.; Paliwal, N.; Damiano, R.J.; Waqas, M.; Nagesh, S.S.V.; Rajabzadeh-Oghaz, H.; Vakharia, K.; Siddiqui, A.H.; Meng, H. Evaluation of Two Fast Virtual Stenting Algorithms for Intracranial Aneurysm Flow Diversion. *Curr. Neurovasc. Res.* **2020**, *17*, 58–70. [[CrossRef](#)] [[PubMed](#)]
27. Xiang, J.; Damiano, R.J.; Lin, N.; Snyder, K.V.; Siddiqui, A.H.; Levy, E.I.; Meng, H. High-Fidelity Virtual Stenting: Modeling of Flow Diverter Deployment for Hemodynamic Characterization of Complex Intracranial Aneurysms. *J. Neurosurg.* **2015**, *123*, 832–840. [[CrossRef](#)]
28. Janiga, G.; Daróczy, L.; Berg, P.; Thévenin, D.; Skalej, M.; Beuing, O. An Automatic CFD-Based Flow Diverter Optimization Principle for Patient-Specific Intracranial Aneurysms. *J. Biomech.* **2015**, *48*, 3846–3852. [[CrossRef](#)] [[PubMed](#)]
29. Bouillot, P.; Brina, O.; Ouared, R.; Yilmaz, H.; Farhat, M.; Erceg, G.; Lovblad, K.O.; Vargas, M.I.; Kulcsar, Z.; Pereira, V.M. Geometrical Deployment for Braided Stent. *Med. Image Anal.* **2016**, *30*, 85–94. [[CrossRef](#)]
30. Wu, Y.F.; Yang, P.F.; Shen, J.; Huang, Q.H.; Zhang, X.; Qian, Y.; Liu, J.M. A Comparison of the Hemodynamic Effects of Flow Diverters on Wide-Necked and Narrow-Necked Cerebral Aneurysms. *J. Clin. Neurosci.* **2012**, *19*, 1520–1524. [[CrossRef](#)]
31. Cebal, J.R.; Mut, F.; Raschi, M.; Scrivano, E.; Ceratto, R.; Lylyk, P.; Putman, C.M. Aneurysm Rupture Following Treatment with Flow-Diverting Stents: Computational Hemodynamics Analysis of Treatment. *AJNR Am. J. Neuroradiol.* **2011**, *32*, 27–33. [[CrossRef](#)] [[PubMed](#)]
32. Tong, X.; Shan, Y.; Leng, X.; Chen, J.; Fiehler, J.; Siddiqui, A.H.; Hu, X.; Liu, A.; Xiang, J. Predicting Flow Diverter Sizing Using the AneuGuide TM Software: A Validation Study. *J. Neurointerv. Surg.* **2023**, *15*, 57–62. [[CrossRef](#)]
33. Fujimura, S.; Brehm, A.; Takao, H.; Uchiyama, Y.; Karagiozov, K.; Fukudome, K.; Yamamoto, M.; Murayama, Y.; Psychogios, M.N. Hemodynamic Characteristics and Clinical Outcome for Intracranial Aneurysms Treated with the Derivo Embolization Device, a Novel Second-Generation Flow Diverter. *World Neurosurg.* **2021**, *159*, e252–e259. [[CrossRef](#)] [[PubMed](#)]
34. Goertz, L.; Dorn, F.; Kraus, B.; Borggrefe, J.; Forbrig, R.; Schlamann, M.; Liebig, T.; Turowski, B.; Kabbasch, C. Improved Occlusion Rate of Intracranial Aneurysms Treated with the Derivo Embolization Device: One-Year Clinical and Angiographic Follow-Up in a Multicenter Study. *World Neurosurg.* **2019**, *126*, e1503–e1509. [[CrossRef](#)]
35. Akgul, E.; Onan, H.B.; Akpınar, S.; Balli, H.T.; Aksungur, E.H. The DERIVO Embolization Device in the Treatment of Intracranial Aneurysms: Short- and Midterm Results. *World Neurosurg.* **2016**, *95*, 229–240. [[CrossRef](#)] [[PubMed](#)]
36. Kaschner, M.G.; Petridis, A.; Turowski, B. Single-Center Experience with the New Generation Derivo Embolization Device in Ruptured Dissecting and Blister Aneurysms. *Acta Radiol.* **2020**, *61*, 37–46. [[CrossRef](#)]
37. Stahl, J.; Marsh, L.M.M.; Thormann, M.; Ding, A.; Saalfeld, S.; Behme, D.; Berg, P. Assessment of the Flow-Diverter Efficacy for Intracranial Aneurysm Treatment Considering Pre- and Post-Interventional Hemodynamics. *Comput. Biol. Med.* **2023**, *156*, 106720. [[CrossRef](#)]
38. Fernandez, H.; Macho, J.M.; Blasco, J.; Roman, L.S.; Mailaender, W.; Serra, L.; Larrabide, I. Computation of the Change in Length of a Braided Device When Deployed in Realistic Vessel Models. *Int. J. Comput. Assist. Radiol. Surg.* **2015**, *10*, 1659–1665. [[CrossRef](#)]
39. Janiga, G.; Rössl, C.; Skalej, M.; Thévenin, D. Realistic Virtual Intracranial Stenting and Computational Fluid Dynamics for Treatment Analysis. *J. Biomech.* **2013**, *46*, 7–12. [[CrossRef](#)]
40. Durka, M.J.; Wong, I.H.; Kallmes, D.F.; Pasalic, D.; Mut, F.; Jagani, M.; Blanco, P.J.; Cebal, J.R.; Robertson, A.M. A Data-Driven Approach for Addressing the Lack of Flow Waveform Data in Studies of Cerebral Arterial Flow in Older Adults. *Physiol. Meas.* **2018**, *39*, 015006. [[CrossRef](#)]

41. Saalfeld, S.; Voß, S.; Beuing, O.; Preim, B.; Berg, P. Flow-Splitting-Based Computation of Outlet Boundary Conditions for Improved Cerebrovascular Simulation in Multiple Intracranial Aneurysms. *Int. J. Comput. Assist. Radiol. Surg.* **2019**, *14*, 1805–1813. [[CrossRef](#)]
42. Xiang, J.; Tutino, V.M.; Snyder, K.V.; Meng, H. CFD: Computational Fluid Dynamics or Confounding Factor Dissemination? The Role of Hemodynamics in Intracranial Aneurysm Rupture Risk Assessment. *AJNR Am. J. Neuroradiol.* **2014**, *35*, 1849–1857. [[CrossRef](#)]
43. Chalouhi, N.; Tjoumakaris, S.I.; Gonzalez, L.F.; Hasan, D.; Pema, P.J.; Gould, G.; Rosenwasser, R.H.; Jabbour, P.M. Spontaneous Delayed Migration/Shortening of the Pipeline Embolization Device: Report of 5 Cases. *AJNR Am. J. Neuroradiol.* **2013**, *34*, 2326–2330. [[CrossRef](#)]
44. Ma, D.; Dargush, G.F.; Natarajan, S.K.; Levy, E.I.; Siddiqui, A.H.; Meng, H. Computer Modeling of Deployment and Mechanical Expansion of Neurovascular Flow Diverter in Patient-Specific Intracranial Aneurysms. *J. Biomech.* **2012**, *45*, 2256–2263. [[CrossRef](#)]
45. Berg, P.; Daróczy, L.; Janiga, G. Virtual Stenting for Intracranial Aneurysms. In *Computing and Visualization for Intravascular Imaging and Computer-Assisted Stenting*; Elsevier: Amsterdam, The Netherlands, 2017; pp. 371–411.
46. Dholakia, R.; Sadasivan, C.; Fiorella, D.J.; Woo, H.H.; Lieber, B.B. Hemodynamics of Flow Diverters. *J. Biomech. Eng.* **2017**, *139*, 021002. [[CrossRef](#)]
47. Kulcsár, Z.; Augsburger, L.; Reymond, P.; Pereira, V.M.; Hirsch, S.; Mallik, A.S.; Millar, J.; Wetzel, S.G.; Wanke, I.; Rüfenacht, D.A. Flow Diversion Treatment: Intra-Aneurismal Blood Flow Velocity and WSS Reduction Are Parameters to Predict Aneurysm Thrombosis. *Acta Neurochir.* **2012**, *154*, 1827–1834. [[CrossRef](#)] [[PubMed](#)]
48. Berg, P.; Voß, S.; Saalfeld, S.; Janiga, G.; Bergersen, A.W.; Valen-Sendstad, K.; Bruening, J.; Goubergrits, L.; Spuler, A.; Cancelliere, N.M.; et al. Multiple Aneurysms AnaTomy CHallenge 2018 (MATCH): Phase I: Segmentation. *Cardiovasc. Eng. Technol.* **2018**, *9*, 565–581. [[CrossRef](#)] [[PubMed](#)]
49. Mariotti, A.; Boccadifuoco, A.; Celi, S.; Salvetti, M.V. Hemodynamics and Stresses in Numerical Simulations of the Thoracic Aorta: Stochastic Sensitivity Analysis to Inlet Flow-Rate Waveform. *Comput. Fluids* **2021**, *230*, 105123. [[CrossRef](#)]
50. Bozzi, S.; Morbiducci, U.; Gallo, D.; Ponzini, R.; Rizzo, G.; Bignardi, C.; Passoni, G. Uncertainty Propagation of Phase Contrast-MRI Derived Inlet Boundary Conditions in Computational Hemodynamics Models of Thoracic Aorta. *Comput. Methods Biomech. Biomed. Eng.* **2017**, *20*, 1104–1112. [[CrossRef](#)] [[PubMed](#)]

Disclaimer/Publisher’s Note: The statements, opinions and data contained in all publications are solely those of the individual author(s) and contributor(s) and not of MDPI and/or the editor(s). MDPI and/or the editor(s) disclaim responsibility for any injury to people or property resulting from any ideas, methods, instructions or products referred to in the content.